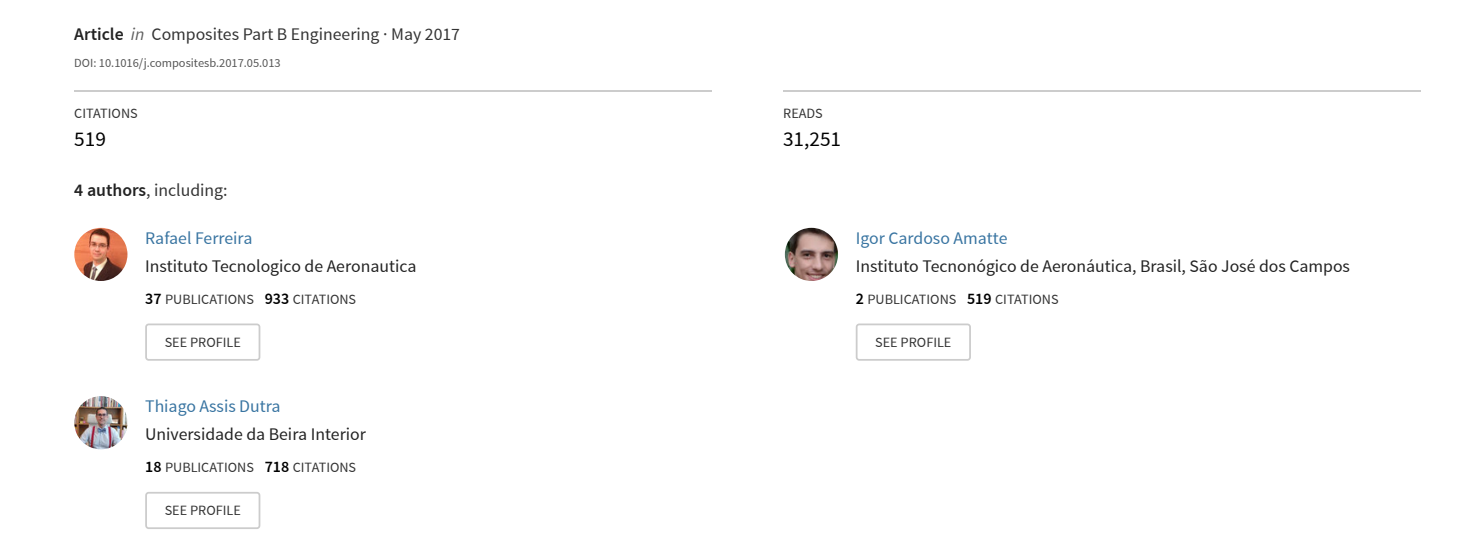
Experimental characterization and micrography of 3D printed PLA and PLA reinforced with short carbon fibers



Experimental characterization and micrography of 3D printed PLA and PLA reinforced with short carbon fibers

Rafael Thiago Luiz Ferreira^{1*}

Igor Cardoso Amatte¹ Daniel Bürger^{2,3} Thiago Assis Dutra¹

September 15, 2017

- ¹ ITA Aeronautics Institute of Technology, GPMA Research Group on Additive Manufacturing, DCTA ITA IEM, 12228-900, São José dos Campos, São Paulo, Brazil
- ² IAE Institute of Aeronautics and Space, AMR Materials Division, DCTA IAE AMR, 12228-900, São José dos Campos, São Paulo, Brazil
 - ³ FAB Brazilian Air Force
 - * rthiago@ita.br. +55 12 3947 6976

Abstract

The objective of this work is the mechanical characterization of materials produced by 3D printing based on fused filament fabrication (FFF, analogous to FDM®). The materials chosen are a polylactic acid (PLA) and a PLA reinforced with short carbon fibers in a weight fraction of 15% (PLA+CF). In view of the FFF nature, which produces specimens layer by layer and following predefined orientations, the main assumption considered is that the materials behave like laminates formed by orthotropic layers. If the 3D printing is made in the 1-2 plane, where 1 is the deposition direction and 2 is a direction perpendicular to 1, the mechanical properties obtained are the tensile moduli E_1 and E_2 , the Poisson ratios ν_{12} and ν_{21} , the shear modulus G_{12} and related strength properties. For this purpose, only unidirectional or specially oriented specimens are used. After tests up to material failure, scanning electron microscopy (SEM) is employed to observe fracture surfaces. It was noticed that, in the microstructure of the PLA+CF, the short carbon fibers stay highly oriented with the material deposition direction in the FFF specimens. This fact, and the also observed length of the fibers, explains differences in material properties encountered among the performed experiments.

Keywords: 3D printing, composite material filament, experimental properties

1 Introduction

3D printing is an established technology for shape prototyping which is gaining ground in the production of functional components. Applications are emerging in several fields at a rapid pace. Examples follow. In agriculture, where equipments and tools for small farms were produced on-site by low cost printers [1]. In biomedical [2, 3], orthotic and prosthetic devices, e.g. in [4] where a printed orthosis was developed for treatment in newborns of developmental dysplasia of the hip. In unmanned aerial vehicles (UAVs), like reviewed in [5] and seen in [6], where a 3D printed component for a multi-rotor aircraft was designed. In bioprinting, where bioinks are 3D printed to develop constructs with biological functions, able to be used in substitution of organs and tissues [7, 8]. In membrane (selective barriers) technology, like described in the review [9] and references therein. There are also examples in aerospace [10, 11], civil engineering [12, 13, 14], metal matrix composites [15, 16, 17], multi material components [18], food production [19] and others [20].

In 3D printing, a technique commonly employed for components of some mechanical responsibility is the fused filament fabrication (FFF), which is the focus of this paper and analogous to fused deposition modeling (FDM®, trademark of Stratasys) [21, 22]. In FFF, which is an additive manufacturing process, thin lines of fused material are deposited side by side and upon each other to form a printed

object. The printers that work in this technique are fed with a filament of thermoplastic printing material. This filament is melted by an extrusion nozzle which is attached to a tridimensional positioning system. The nozzle is controlled to perform a selective material deposition that generates the geometry of the desired component. For instance, the mechanical characteristics of FFF 3D printed materials depend on several build parameters [23, 24, 25], like the fused line deposition height, width and orientation, type of internal microstructure, extrusion temperature and presence and configuration of external walls.

Common and not expensive printing materials are the polymers ABS (acrylonitrile butadiene styrene) and PLA (polylactic acid). Other polymers employed in FFF are the PETG (polyethylene terephthalate glycol-modified), Nylon (a kind of polyamide), PEEK (polyether ether ketone) and PEI (polyethylenimine), each one with particular capabilities. For example, a special PEI from the company 3DXtech has a higher strength and is suited to aeronautical applications, since it is flame retardant and has low smoke emission when burned.

Despite the variety of printing polymers available, their mechanical properties of stiffness and strength are naturally lower than those of other traditional engineering materials employed in high performance applications, like metals and fiber composites. Moreover, the FFF process generates void spaces between material deposition lines, which even lowers those properties, also limiting the applicability of printed components.

In order to broaden the capabilities of FFF materials, research on polymer matrix reinforced composites for 3D printing has recently grown. Examples are polymers reinforced by ceramics like Al_2O_3 and SiC [26, 27, 28] and also stiff fibers like carbon, glass and kevlar [29, 30, 31, 32]. An extensive review on 3D printing of polymer matrix composites, including several technologies and applications, is presented in [33]. This review permits to conclude that very important improvements were achieved on the subject in recent years, and they permit to expand the applicability of printed materials into functional components. However, this applicability is still limited. With continuous research and increasing interest on 3D printing, it can be foreseen that higher gains will happen in the near future.

1.1 Motivation

In view of the exposed, the motivation of the present research work is to experimentally obtain mechanical properties of 3D printed materials: a PLA basic material and a composite version reinforced with short carbon fibers, henceforth called PLA+CF. The quantities of interest are tensile properties at two perpendicular directions and also shear properties, considering stiffnesses and strengths. The acquired data will be assessed in such a way they can be further employed in the design of 3D printed components and materials development.

Several authors have recently devoted themselves to determine 3D printed material properties via experiments, inclusive for new FFF composites and considering aspects of the FFF process. The following literature review in Sec.1.2 discusses contributions in this line of thought. After that, it is considered the definition of the present work objectives in Sec.1.3 and the original experimental contributions in Sec.1.4.

1.2 Literature review

In [34], the effect of FFF build parameters on the final mechanical properties of ABS printed specimens was investigated by means of experimental characterization. The selected build parameters were: deposition line width, air gap between lines, extrusion temperature, printing orientation and the color of the filament. In tensile testing, it was verified that deposition line width and printing orientation presented more significant effects on the final mechanical properties, in accordance to [23]. For the compression investigation, only the print direction was evaluated. In this case, the compression strength was higher than the tensile strength. In [24], the influence of printing parameters in mechanical properties of FFF specimens was studied with the aid of experiments and response surfaces, also used in final properties optimization. A review on the influence of FFF parameters in resultant material properties is shown in [25].

A methodology for mechanical properties characterization of FFF parts based on classical lamination theory (CLT) was presented in [35]. The experimental investigations were conducted on ABS printed parts. Both the bulk feeding filament and a thin filament extruded in a 3D printer were tested, together with standardized test specimens. The tensile strength and elastic modulus for both ABS feeding filament and ABS printed filament were similar, but the maximum strain was notably affected by the FFF process. Analogously as observed in [34], it was verified that the printing orientation affects the resulting mechanical properties. Recently, this fact was also investigated in yielding of 3D printed materials by [36] and [37]. The latter used CLT and Tsai-Hill yield criterion to successfully model the strength behavior of specimens 3D printed at several orientations.

In [29], experiments were performed in order to investigate the effect of including short glass fibers in an ABS filament for use as 3D printing feeding material. Specimens with different volume fractions of glass fiber were manufactured by FFF and tested. It was verified that short glass fibers improved the strength of the ABS filament, although the flexibility was reduced. In addition, the effects of adding a small amount of plasticizer and compatibilizer was also investigated, showing for this case an improvement on the flexibility. It was also determined an appropriate fiber content that achieves a compromise between processing and resulting mechanical properties.

In [38], the resulting mechanical properties of short carbon fiber-containing ABS specimens were determined, at different fiber content and manufactured by both the FFF and injection molding processes. The addition of short carbon fibers to ABS increased the strength and the elastic modulus for both FFF and injection molding parts. The FFF samples presented a void content higher than injection molding samples, as could be seen on SEM micrography. Another remark is related to the weak adhesion between fibers and matrix. [39], short carbon fibers were added to ABS in a weight fraction of 13% and test specimens were produced by FFF, oriented with the x direction on the printing bed plane and in the perpendicular z direction out of this plane. The addition of fibers improved stiffness and strength of specimens printed according to x, but strength was diminished for z-printed samples due to poor fused material adhesion in that direction.

In [31], the effects of short carbon fiber content and length were evaluated on the mechanical properties of ABS composite specimens, manufactured by the FFF process. It could be verified that there is a limit to increase the tensile strength while increasing the fiber content. From that point, the tensile strength was reduced while increasing the fiber content, presenting values similar to those of pure thermoplastic. The effects on elastic modulus presented a behavior similar to that for tensile strength, however the smallest value was found for the pure thermoplastic sample. The specimens manufactured with longer carbon fibers presented larger tensile strengths and elastic moduli in comparison to that with shorter carbon fibers. Regarding to the infill pattern deposition directions, the layers were not printed oriented with the tensile testing direction but at $\pm 45^{\circ}$. An extension of this study was presented in [40], where tensile properties of a composite of ABS and short carbon fibers were investigated under the influence of several printing parameters: deposition line orientation, infill speed, nozzle temperature and layer thickness. However, unidirectionally printed specimens were again not employed.

In [41], 3D printed PLA reinforced with the posterior addition of pre-stressed long natural fibers [42] was submitted to tensile and flexural tests. The reinforcing pre-stressed fibers increased the material stiffness in both load cases in comparison to the PLA without those fibers.

In [43], PLA reinforced with continuous carbon fibers was manufactured by 3D printing and tested for mechanical and thermodynamic properties. Such composite was produced in a common version and in a modified version with an additive for PLA and fibers with special surface treatment, aiming to improve fiber-matrix adhesion. Tensile and flexural mechanical tests were performed, indicating that the modified composite performed better with respect to flexural and tensile strengths. Previously, [44] also pointed this trend working in molded specimens of a composite of PLA and ramie natural fibers, obtaining improved results for tensile, flexural and impact strengths when working with specially treated fibers. In [45], it was evaluated a FFF 3D printed PLA reinforced with continuous carbon fibers, also leading to strength increase in bending and tensile tests. It was also shown that the employed reinforcement permitted to obtain high strengths while decreasing parts fill density, thus saving weight. A production process, based on FFF, for 3D printing PLA reinforced with continuous carbon fibers was investigated in [46].

In [47], 3D printed PLA reinforced with continuous carbon fibers was recycled and the materials

obtained were used again in the FFF 3D printing of a new PLA composite with continuous carbon fibers. Tensile and flexural experiments showed that the recycled material performed better than the virgin one with respect to strengths. The reason behind this behavior is the residual impregnation of PLA in the recycled fibers that enhanced fiber-matrix adhesion.

In [48], 3D printed specimens of nylon reinforced with continuous kevlar fibers were tested in several volume fractions. The fibers were practically oriented with the test direction. Results show increase of stiffnesses and strengths with increase of fiber volume content. It was also proposed a volume averaging stiffness method that is able to predict stiffnesses of 3D printed composite parts of that particular case, with reasonable agreement with experimental data. The same process utilized in [48] was employed in [30] to 3D print tensile test specimens of nylon reinforced with continuous carbon fibers, in different fiber volume fractions. The tests results were promising for the samples with higher fiber volume fractions, where tensile strengths values were close to those found in some traditional thermo-set carbon fiber composites.

In [49], ABS reinforced with carbon nanofibers of length about $100\mu m$ was tested in several printing orientations. The results show consistent increase of stiffness and strength for the reinforced material, whose gains varied with printing orientation. Molded PLA reinforced with carbon nanofibers was experimentally evaluated in [50]. Weight fractions of 1, 3, 5, 10 and 15% of nanofibers content were investigated. Using nanofibers of length below $4\mu m$, it was reported that the tensile modulus of the composites increased with nanofibers weight fraction. With 15% of nanofibers, the tensile modulus obtained for the PLA composite was more than twice of the pure thermoplastic. Tensile strength varied a little with nanofibers weight fractions, due to the reported excessive fiber pull outs and poor matrix adhesion.

1.3 Objective

The objective of this work is to experimentally characterize a PLA basic material and a PLA reinforced with short carbon fibers (PLA+CF). This composite has a weight fraction of 15% of carbon fibers whose length was estimated in about 60 μm .

The mechanical properties obtained by tests are those respective to the plane of deposition during 3D printing. If this plane is the 1-2, where 1 is the direction of deposition and 2 is a direction perpendicular to this direction of deposition, the mechanical properties to be obtained are the tensile moduli E_1 and E_2 , the Poisson ratios ν_{12} and ν_{21} , the shear modulus G_{12} and the strength properties related to these stiffnesses.

For this purpose, only unidirectional or specially oriented specimens are employed, printed at 0° , 90° and $\pm 45^{\circ}$, being tested up to failure. As there are not specific test standards for printed materials, the ASTM D638-10 [51] and ASTM D3518-13 [52] are followed in adaptation. After that, scanning electron microscopy (SEM) is conducted to analyze the specimens fracture surfaces. The micrographs obtained revealed microstructural details in terms of fiber orientations and fiber lengths, which explain differences found in stiffness and strength properties evaluated from experimental data.

1.4 Contribution

Regarding to the contribution of the present study, it is shown a mechanical characterization of PLA reinforced with short carbon fibers with a comparison to single PLA properties, which is not found in the literature. This is found for ABS with short fibers [29, 49, 38, 39, 31, 40], Nylon with continuous/long fibers [30, 48], PLA with continuous/long fibers [41, 43, 45, 46, 47], PLA with carbon nanofibers [50] and other PLA composites [53, 54, 55].

Moreover, this work presents the testing of shear properties in 3D printed specimens, which was not also found in previous works for any printing material. The most usual tests are tensile and flexural [56, 43, 50, 46, 47, 45], which permit to determine tensile stiffness properties. Besides, Poisson ratios are here documented, which is seldom seen in the literature.

Finally, this study shows new results for tensile properties in a direction perpendicular to that of material deposition, for 3D printed PLA with short carbon fibers. In the literature, the usual is to characterize materials only along the printing direction [41, 43, 47, 46] or without specimens carefully

oriented with the test direction [31, 40] (although it is well documented the influence of printing orientation in the properties of FFF produced specimens [34, 23, 35]). It has to be mentioned that [34] tested ABS in several directions, including the printing and the perpendicular to printing, and [39] tested ABS reinforced with short carbon fibers in a direction out of the plane of printing.

Table 1 contextualizes the present experimental contribution in view of works cited in the review of Sec.1.2. The results of this study imply that there exist differences between tensile and shear properties of PLA and PLA+CF, here evaluated and documented in a way not seen in the literature. They have application in design of components produced by 3D printing, in general developments of FFF composites and tensile and shear testing of these materials.

2 Methodology of mechanical characterization

2.1 Main assumption and specimen printing orientations

The experiments here performed were made under the assumption that the test specimens behave like laminated materials [57], made by orthotropic layers whose principal direction of highest stiffness is the printing orientation direction. This can be assumed due to some facts. At first, specimens were 3D printed only using rectilinear infill with volume fraction of 100%, which means that fused material lines were deposited only parallel to each other, forming layers which are placed on top of each other to build a specimen. Second, the layers followed only specific orientations: 0° , 90° and $\pm 45^{\circ}$, as illustrated in Fig.1. Finally, the 3D printing parameters of deposition line height and width were kept the same in all specimens. Therefore, it is possible to think that the experiments were all made upon a material of constant microstructure, placed at specific orientations, following the FFF deposition.

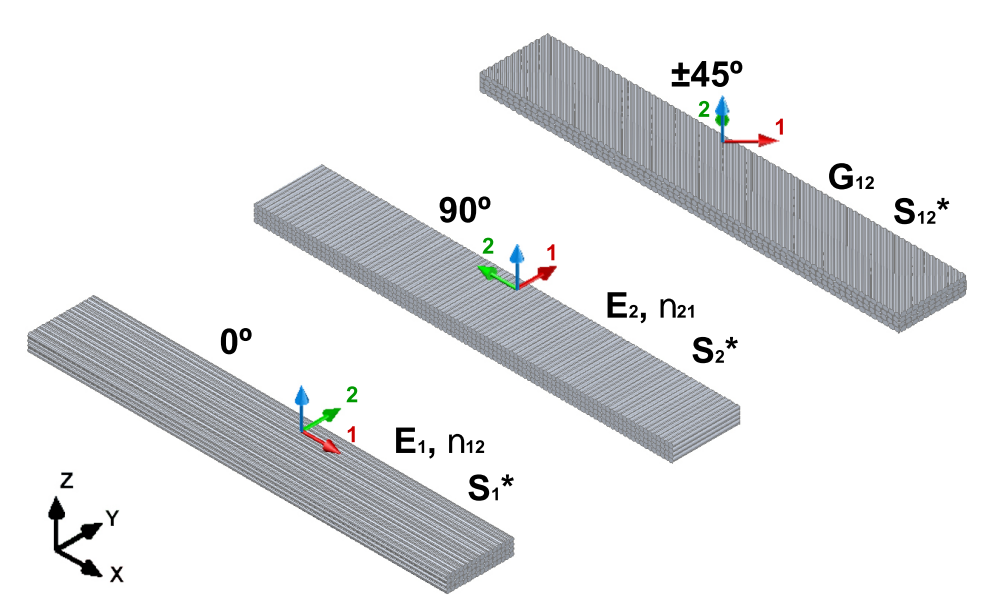


Figure 1: Illustration of printing orientations (0°, 90° and $\pm 45^{\circ}$). The local material directions are 1, the direction of printing, and 2, perpendicular to 1. The global coordinates are x,y,z.

2.2 Measured material characteristics

Specific material characteristics were measured, respective to the 1-2 material plane in Fig.1, using specially oriented specimens. The 1-2 plane is the same of 3D printing. The 1 is the direction of FFF line deposition and 2 is the direction perpendicular to this line deposition. The 1 and 2 are local material directions. From the specimens oriented at 0° , the tensile modulus in the deposition direction E_1 , the Poisson ratio ν_{12} and the tensile strength S_1^* were determined. From the specimens oriented

pers.	Besilts
recent pa	Flor Tests
d very	Axial/
previous an	Shear Tests
compared to	
resent contribution compared to previous and very recent papers.	FFF Param PO
Table 1: Present con	Process
Table	forc a

		Table	e I. riese	ne continuation	л сошрагес	i to previous a	table 1: riesent contribution compared to previous and very recent papers.	Jers.	
Paper	Matrix	Reinforc. a	Process	FFF Param.	РО	Shear Tests	Axial / Flex Tests Results ^{b}	$\operatorname{Results}^b$	Comments
Zhong et al.,	ABS	GF short	FFF,	TE 250,	[0],[0]		Tensile,	S_*	Tests fiber weight fractions
2001 [29]			IM	1 C 60			no standard		(15 to 20%). Unidirec. tests
									in two perpendicular PO.
Ahn et al.,	$^{ m ABS}$		FFF,	Several AG,	[0], [90],		ASTM D3039	S^*, S^*_c	Unidirec. tests in two
2002 [34]			IM	DLH, DLW,	[0/90]		(tensile) & D695		perpendicular PO. Tests
				TE and MC	[45/-45]		(compression)		influence of FFF param.
Bellini and	ABS		FFF	N/A	06 0]		ASTM D5937-96	$E, S^*,$	
Güçeri,					45 -45],		(tensile) $\&$	S_{fl}^*	
2003 [35]					random		D790-96 (flexural)	,	
Shofner et al.,	ABS	CF short	FFF	N/A	several		ASTM D638	E, S^*	
2003 [49]		$(\mathrm{FL}\ 100\ \mu m)$					(tensile)		
Tekinalp et al.,	ABS	CF short	FFF,	TE 205,	[0]		ASTM D638	E, S^*	Tests fiber weight fractions
2014 [38]		$(FL\ 200)$	$_{ m IM}$	TB 85,			(tensile)		(10 to 40%).
		to 400)		DLH 0.2					
Love et al.,	ABS	CF short	FFF	DLH 0.254	[0] and		ASTM D638	E, S^*	Tests properties out of
2014 [39]					out of plane		(tensile)		printing plane.
Ning et al.,	$^{ m ABS}$	CF short	FFF	TE 230,	[45/-45]		ASTM D638-10	$E, S^*,$	Evaluates several material
2015 [31]		$(FL\ 100)$		DLH 0.2			(tensile) $\&$	$E_{fl}, S_{fl}^*,$	constants and fiber weight
		and 150)					D790-10 (flexural)	others	fractions $(3 \text{ to } 15\%)$.
Ning et al.,	$^{ m ABS}$	CF short	FFF	Several TE	[0/90],		ASTM D638-10	E, S^*	Tests influence of FFF
2016 [40]				and DLH	[45/-45]		(tensile)		parameters on properties.

^aAcronyms: AG air gap, CF carbon fiber, DLH deposition line height (mm), DLW deposition line width (mm), FFF fused filament fabrication, FFF* process adapted from FFF, FL fiber length (μm) , GF glass fiber, IM injection molding, MC material color, N/A not available, NF natural fibers, PO printing orientation (°), TB bed temperature (°C), TC chamber temperature (°C), TE extrusion nozzle temperature (°C).

^bResults: E tensile modulus, E_{fl} flexural modulus, G_{fl} in-plane shear modulus, G_{fl} tensile strength, G_{fl} compression strength, G_{fl} flexural strength, G_{fl}

Poisson ratio.

Table 1: (Continued) Present contribution compared to previous and very recent papers.

			- 11	/		· ·	, , , , , , , , , , , , , , , , , , ,	7 7	
Paper	Matrix	Reinforc. a	$_{\rm Process}$	FFF Param.	РО	Shear Tests	Axial / Flex Tests	Results^b	Comments
Melenka et al.,	Nylon	Kevlar	FFF*	DLH 0.1	[0]	ı	ASTM D638-14	E, S^*	Uses a process adapted
2016 [48]		cont.			(fibers)		(tensile)		from FFF.
Klift et al.,	Nylon	CF	FFF*	DLH 0.125	[0]		JIS K 7073	E, S^*	Tests different fiber
2016 [30]		cont.			(fibers)		(tensile)		volume fractions.
Anwer and	PLA	CF nano	IM			1	ASTM D638	$E, S^*,$	Tests weight fractions (1 to
Naguib,		(FL					(tensile)	others	15%), thermal and
2016 [50]		$< 4\mu m)$							dynamical properties.
Jaszkiewicz	PLA	GF and	IM		1		EN ISO 579	S_*	Investigates
et al., 2016		NF short					(tensile)		processability of
[53]									short NF and GF.
Li et al.,	PLA	CF	FFF*		[0]		Tensile,	E, S^*	Uses a new process
2016 [43]		cont.					no standard		adapted from FFF.
Tian et al.,	PLA	CF	FFF*	Several TE	[0]	ı	ISO 14125:	E_{fl}, S_{fl}^*	Uses a process adapted
2016 [46]		cont.		and DLH			1998 (flexural)	•	from FFF, investigates
									several parameters.
Tian et al.,	PLA	CF	FFF*	TE 240	[0]		GB/T 1447:2005	$E, S^*,$	Uses a process adapted
2017 [47]		cont.					(tensile) & 1449:	$E_{fl}, S_{fl}^*,$	from FFF w/ recycled CF.
							2005 (flexural)	others	Evaluates impact properties.
Yao et al.,	PLA	CF	FFF*	TE 205,	[0]	1	ISO 527-4:1997	$S^*, S^*_{fl},$	Investigates CF in
2017 [45]		cont.		TB 60			(tensile) &	$^{ m others}$	structural-health
							14125:1998 (flex.)		monitoring.
Present	PLA	CF	FFF	TE 190,TB 70	[0],	ASTM	ASTM D638-10	$E, S^*,$	Unidirec. tests in two
Contribution		$_{ m short}$		DLH 0.3,	[90],	D3518-13	(tensile)	$G, S_s^*,$	perpendicular PO. Shear
		(FL 60)		DLW 0.33	[45/-45]	(shear)		ν	prop. and Poisson ratios

at 90°, the tensile modulus perpendicular to the deposition direction E_2 , the Poisson ratio ν_{21} and the tensile strength S_2^* were determined. From the specimens oriented at $\pm 45^\circ$, the shear modulus at the 1-2 plane G_{12} and the shear strength S_{12}^* were determined. Five specimens per sample were tested for each one of the three orientation cases and for each printing material (PLA and PLA+CF), totalizing 30 test runs.

2.3 Standards for specimens and printing parameters

Based on the authors' best information there are not, up to now, specific standards for testing materials produced by the FFF method. Here, standards for polymers and laminated composite materials were followed in adaptation, as the example of other authors [58, 59]. For the determination of stiffness and strength properties at material directions 1 and 2 it was chosen the standard ASTM D638-10 [51], devoted to tensile tests of polymers. The specimen shape employed was the I-type ("dog bone"), with outer length and width respectively of 165 mm and 19 mm, as shown in Fig.2. The nominal thickness was 3.3 mm reached with 11 printed layers, which were deposited either at 0° or 90° along the tensile direction. Therefore, the stacking sequences for the specimens were respectively $[0^{\circ}]_{11}$ and $[90^{\circ}]_{11}$. To obtain the 1-2 plane shear stiffness and strength properties of the printed material, it was used the standard ASTM D3518-13 [52], specific for polymer matrix composite materials. The specimens employed were rectangular and had 25 $mm \times 200 \ mm$, as illustrated in Fig.2. The nominal thickness was 4.8 mm, reached with 16 printed layers whose stacking sequence was $[45^{\circ}/-45^{\circ}]_{4s}$ (symmetric), as imposed by the followed standard.

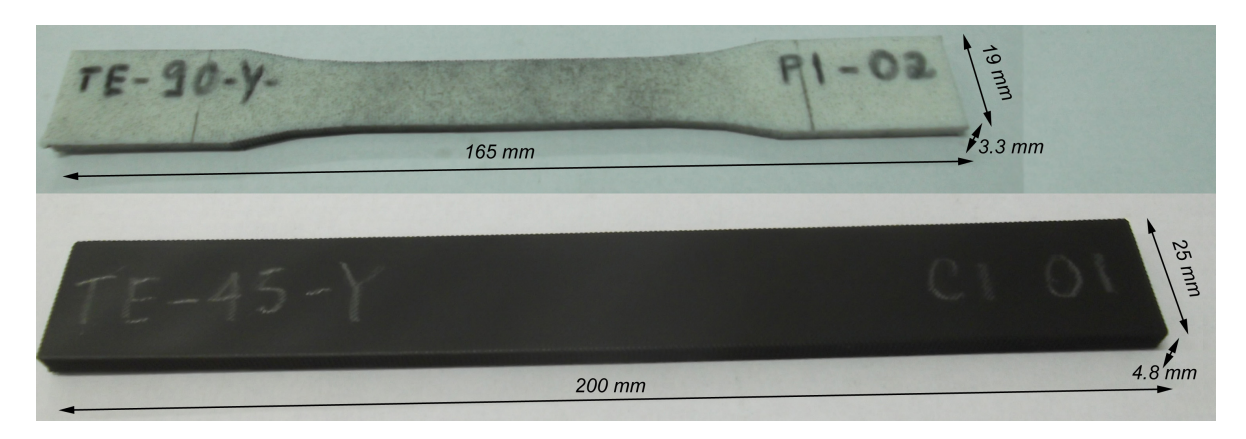


Figure 2: Employed specimens: tensile ("dog bone", upper) and shear (rectangular, lower). They illustrate the tested materials: the white is the PLA and the black is the PLA+CF.

The test specimens were produced with an open source 3D printer BQ Prusa i3 Hephestos, with a printing envelope of 215 $mm \times 210~mm \times 180~mm$, nozzle diameter of 0.4 mm and an adapted MK2a heat bed (see reprap.org) to avoid specimens warping. The printing parameters employed were: nozzle extrusion temperature of $190^{\circ}C$, heat bed temperature of $70^{\circ}C$, deposition line (layer) height 0.3 mm, deposition line width 0.33 mm and printing speed of 3000~mm/min.

2.4 Printing materials

The PLA material used is made by BQ, whose base material is the polylactide resin 9051-89-2, which corresponds to the 4043D commercial designation from NatureWorks, according to both companies data sheets. The PLA+CF is produced by Proto-Pasta, and is made from the 4043D resin reinforced with chopped short carbon fibers in a weight fraction of 15%. Therefore, both are comparable with respect to the addition of reinforcing fibers since the base material is the same. The diameter of the 3D printer filaments employed was 1.75mm.

2.5 Testing equipment

The experiments were performed using an Instron 5500R universal testing machine, with a load cell of capacity of 150 kN. All the specimens were loaded up to material failure at a displacement rate of $1 \ mm/min$. Strains in the specimens were monitored by a video gauge equipment, an iMetrum NR 4QCTWW1 with camera GigE and 201693 lenses, which was able to measure strains in a direction parallel to that of loading and at the same time in a direction perpendicular to that of loading. The data acquisition rate was $10 \ Hz$ for displacements, strains and loads measured. After mechanical testing, some specimens had their fracture surfaces evaluated by scanning electron microscopy (SEM), using an equipment Zeiss Leo 435 VPi.

3 Results for mechanical properties

Figures 3, 4 and 5 show stress-strain curves obtained from the data gathered in the experiments for the PLA and PLA+CF, respectively printed at 0°, 90° and ±45°. They were post-processed in order to obtain the mechanical properties shown in Tab.3, 4 and 5, which collect tensile and shear elastic moduli, Poisson coefficients and strength values encountered for the PLA and PLA+CF.

The tensile properties were calculated in accordance to the standard ASTM D638-10 [51]. The specimens were loaded at the direction x, perpendicular to y, according to Fig.1. The applied load P was measured by a load cell and strains ε_x and ε_y were measured by a video gauge (both equipments described in Sec.2.5). Tensile moduli E_i (E_1, E_2) and Poisson ratios ν_{ij} (ν_{12}, ν_{21}) were calculated by:

$$E_{i} = \frac{\sigma_{x}^{0.25} - \sigma_{x}^{0.05}}{\varepsilon_{x}^{0.25} - \varepsilon_{x}^{0.05}}, \quad \nu_{ij} = \frac{\varepsilon_{x}^{0.25} - \varepsilon_{x}^{0.05}}{\varepsilon_{y}^{0.25} - \varepsilon_{y}^{0.05}}.$$
 (1)

In Eq.(1), ε_x^k are longitudinal normal strains of value k% (close to 0.05% and 0.25% in the case), ε_y^k are transverse normal strains at the level of ε_x^k and σ_x^k are tensile stresses corresponding to ε_x^k . Therefore, both E_i and ν_{ij} are given by chordal values obtained from the data gathered. The tensile stresses σ_x^k are given by:

$$\sigma_x^k = \frac{P^k}{A}.\tag{2}$$

In Eq.(2), P_k is the tensile load at ε_x^k and A is the cross sectional area of a specimen. Finally, considering that P_{max} is the maximum load applied to a specimen, the tensile strengths S_i^* (S_1^*, S_2^*) were calculated by:

$$S_i^* = \frac{P_{max}}{A}. (3)$$

The shear properties were calculated in view of the standard ASTM D3518-13 [52]. Again, the specimens were loaded at the direction x, the applied load P was measured by a load cell and strains ε_x and ε_y were measured by a video gauge. The shear modulus G_{12} was calculated by:

$$G_{12} = \frac{\tau_{12}^{0.6} - \tau_{12}^{0.2}}{\gamma_{12}^{0.6} - \gamma_{12}^{0.2}}.$$
(4)

In Eq.(4), γ_{12}^l are shear strains of value l% (close to 0.2% and 0.6% in the case) and τ_{12}^l are shear stresses corresponding to γ_{12}^l . Therefore, G_{12} is obtained as a chordal modulus. The shear strains γ_{12}^l are calculated using:

$$\gamma_{12}^l = \varepsilon_x^l - \varepsilon_y^l. \tag{5}$$

The Eq.(5) regards the measured strains in the outer layers of the shear specimens (oriented at 45°) and implied coordinate transformation relations. The ε_x^l and ε_y^l are the measured normal strains (longitudinal and transverse, respectively) when γ_{12}^l happens. Based on transformation relations for stresses, the shear stresses τ_{12}^l are given by:

$$\tau_{12}^l = \frac{P^l}{2A}.\tag{6}$$

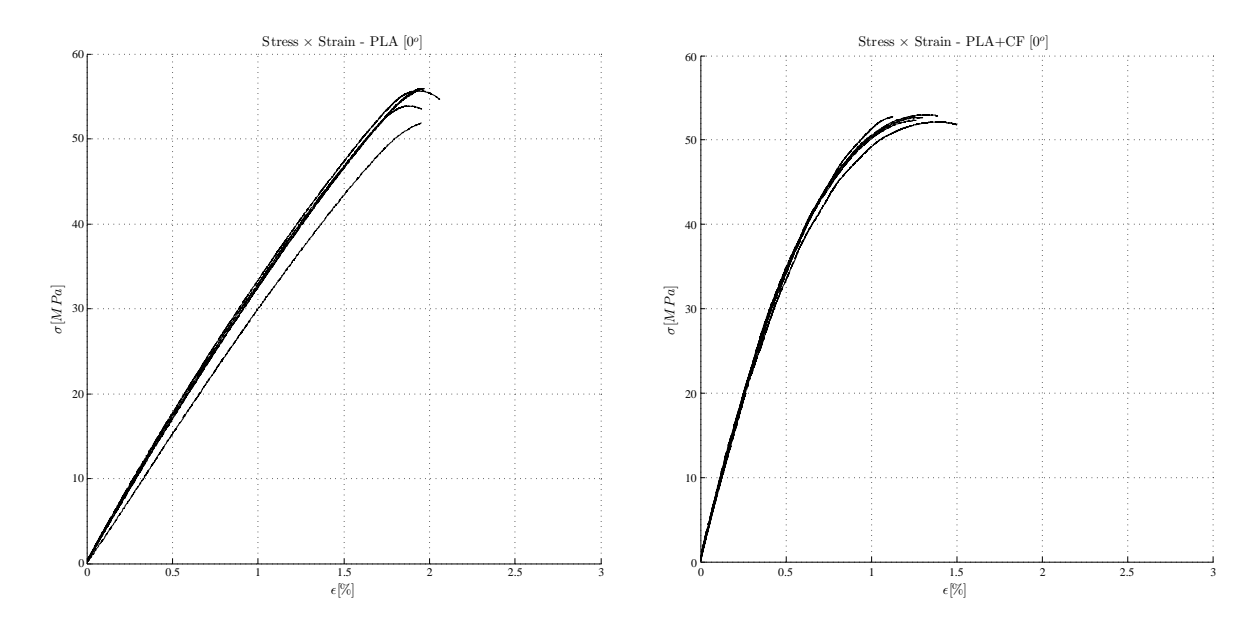


Figure 3: Stress \times strain data for PLA and PLA+CF printed at 0° .

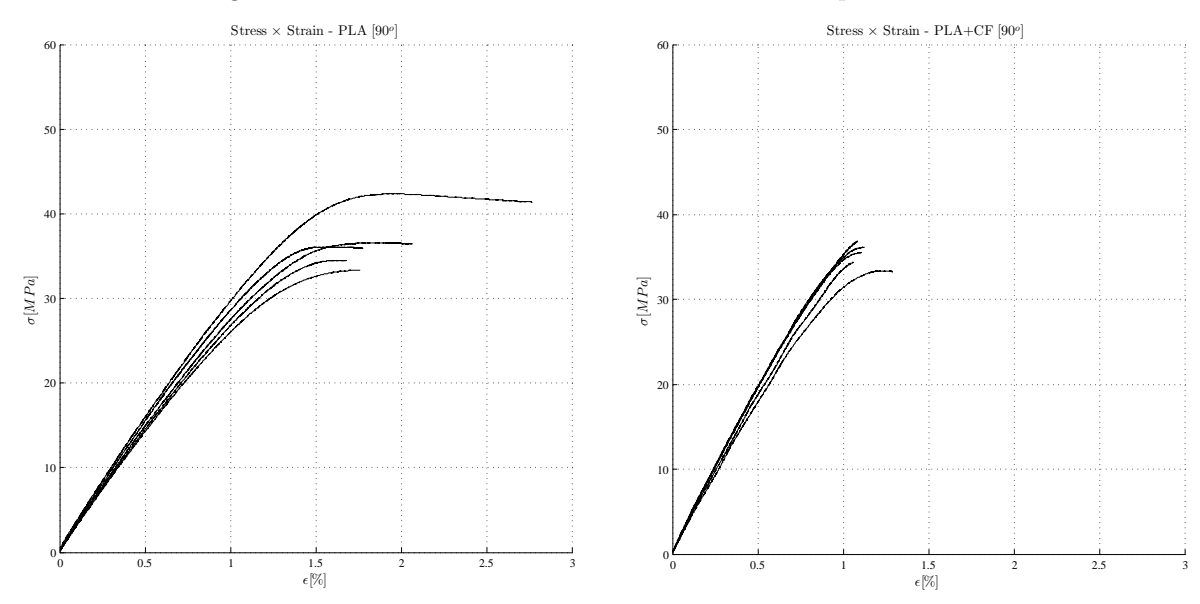


Figure 4: Stress \times strain data for PLA and PLA+CF printed at 90°.

Table 3: PLA and PLA+CF tensile and shear elastic moduli.

PLA PLA+CF ASTM Property Direction Max. Dev. Max. Dev. Standard Avg. Avg. Tensile $0^{\circ} (E_1)$ 3596 3376 212 7665 7541 96 D638Modulus (MPa) $90^{\circ} (E_2)$ 3340312514841453920167In-plane Shear 5 $\pm 45^{\circ} \ (G_{12})$ 1140109236 12701268D3518Modulus (MPa)

	Table 4	: PLA a	and PLA	A+CFF	Poisson (coefficie	$\mathrm{nts.}$	
Droporter	Direction		PLA		I	PLA+Cl	7	ASTM
Property	Direction	Max.	Avg.	Dev.	Max.	Avg.	Dev.	Standard
Poisson	ν_{12}	0.349	0.331		0.408	0.400	0.012	D638
Coefficient	$ u_{21}$	0.336	0.325	0.014	0.163	0.150	0.008	D036

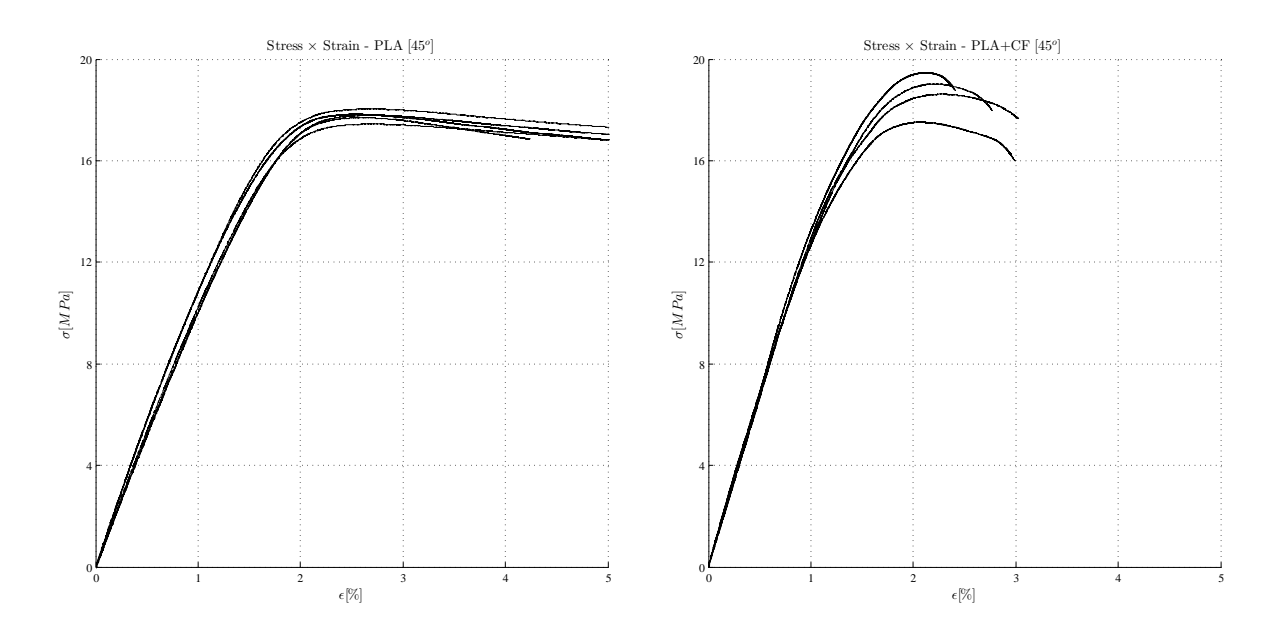


Figure 5: Stress \times strain data for PLA and PLA+CF printed at $\pm 45^{\circ}.$

Table 5: PLA and PLA+CF material strengths.

Duonoutre	Dimention	PLA			PLA+CF			ASTM
Property	Direction	Max.	Avg.	Dev.	Max.	Avg.	Dev.	Standard
Tensile	$0^{\circ} (S_1^*)$	56.1	54.7	1.9	53.7	53.4	0.2	D638
Strength (MPa)	$90^{\circ} \ (S_2^*)$	42.9	37.1	3.5	37.0	35.4	1.5	D036
In-plane Shear Strength (MPa)	$\pm 45^{\circ} \ (S_{12}^*)$	18.3	18.0	0.8	19.6	18.9	0.8	D3518

In Eq.(6), A is the cross-sectional area of the specimen and P^l is the applied load when γ_{12}^l happens. Finally, the shear strength S_{12}^* was calculated using:

$$S_{12}^* = \frac{P_{max}^s}{2A}. (7)$$

In Eq.(7), P_{max}^s is the maximum load at or below γ_{12}^5 (shear strain equal to 5%), as ASTM D3518-13 recommends.

Standard deviations of quantities shown in Tab.3 to 5 were calculated according to their respective base standards.

From the results in Tab.3, it can be seen that the E_1 tensile modulus for the PLA+CF was more than twice (2.2 times) higher than the same property for the PLA, considering the average values. The E_2 tensile modulus for the PLA+CF was about 1.25 times higher than the same property for the PLA, a difference not as big as found for E_1 . The G_{12} in-plane shear modulus for the PLA+CF was about 1.16 times higher than the same property for the PLA, a difference even lower than the found for E_2 . These results show that short carbon fibers provided the highest increase in stiffness for the PLA+CF tested in the printing direction. Besides, it is interesting to notice that E_1 for the PLA is only slightly higher (about 1.08 times) than E_2 for the same material. Therefore, for the PLA, the printing orientation did not influence the material stiffness that much.

Table 4 shows that the Poisson coefficients ν_{12} and ν_{21} found for the PLA were about the same. Contrariwise, these properties were a lot different for the PLA+CF, with ν_{12} about 2.5 times higher than ν_{21} . This can be explained by the differences found for E_1 and E_2 for PLA+CF, which shows that it is much more difficult to stretch the material at the direction 1 (printing direction) than at the direction 2, a typical behavior found in polymer composites reinforced with unidirectional carbon fibers.

From the results in Tab.5, it can be noticed that the material strengths S_1^* , S_2^* and S_{12}^* for the PLA and the PLA+CF were about the same, indicating that the short carbon fibers did not change substantially those properties. Contrariwise, in previous works [31, 38], short carbon fibers improved both stiffness and strength of the polymer ABS. For the PLA+CF here tested, it can be assumed that the ultimate loads were carried out mostly by the matrix material, indicating poor matrix-fiber load transfer at that point. This can be explained by the poor PLA-carbon fiber adhesion, already reported in the literature [43, 47].

However, the PLA+CF had lower strains at failure as can be seen from Fig.3 to 5, indicating a more brittle behavior than that seen in the PLA. It can be said that the short carbon fibers in PLA+CF favored the known naturally brittle behavior [54] of the PLA.

4 SEM of specimens

Scanning electron microscopy (SEM) was used to obtain micrographs of the tested samples fracture surfaces. Four specimens were observed: three for the PLA+CF, each one printed in one of the studied directions 0° , 90° and $\pm 45^{\circ}$, and one for the PLA, printed at 0° . Figures 6 to 14 show the acquired images.

Figures 6 to 8 show, with increasing magnification, the fracture surface of the PLA+CF specimen printed at 0° . In Fig.6, with magnification of $200\times$, it is possible to see details of the printing process, like the cross-sectional shape of the fused deposited lines, their periodicity and the triangular shaped voids left between deposited lines. In Fig.8, with magnification of $3000\times$, the presence of reinforcing short carbon fibers is clear. They show up like grayish cylinders, dispersed over the PLA+CF matrix.

In Fig.7, with magnification of $1000\times$, it is also possible to see the short carbon fibers in PLA+CF, which are the grayish dots inserted in the PLA matrix. Still in Fig.7, it is possible to notice some voids (darker dots) which have the same shape of the short carbon fibers cross sections. These voids were left by fiber pull-outs during failure of the specimen in the tensile test. Moreover, in Fig.7 and 8, other porosities which are not due to fiber pull-outs are also noticeable. In [31], the appearance of such voids is also reported while working with ABS, and is there explained as being left by gas escaping during printing. However, the exact reason that caused their appearance in PLA is not known by the present authors.

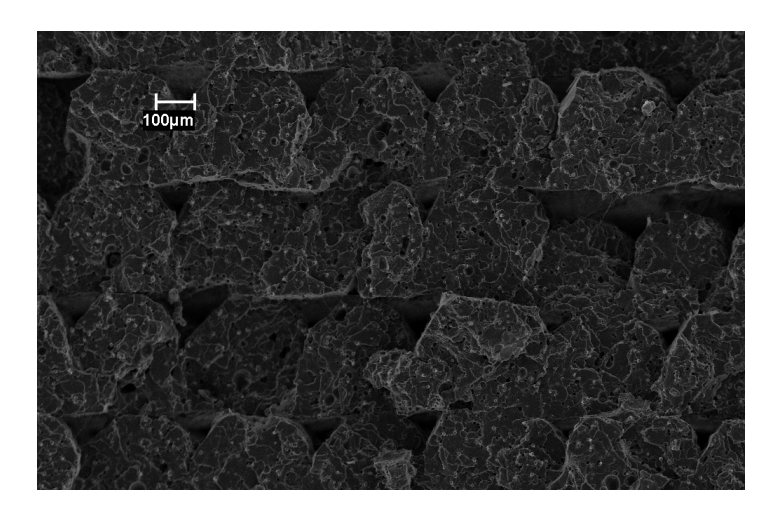


Figure 6: Specimen of PLA+CF at 0° magnified $200 \times$.

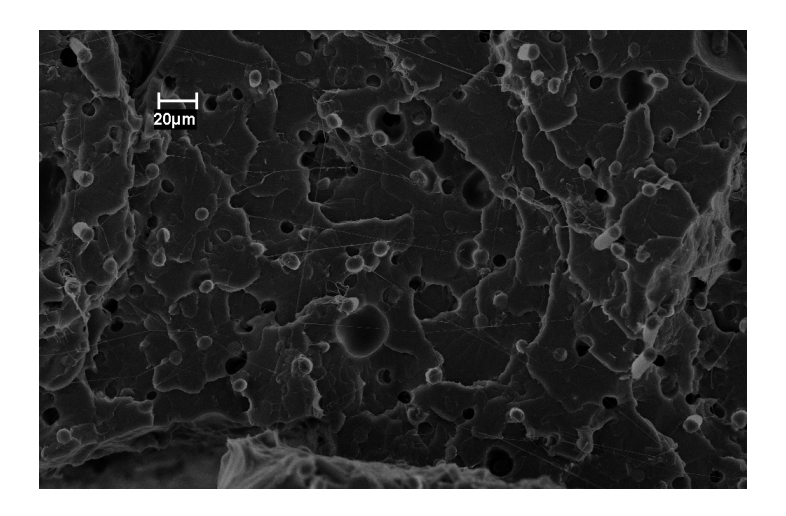


Figure 7: Specimen of PLA+CF at 0° magnified $1000 \times$.

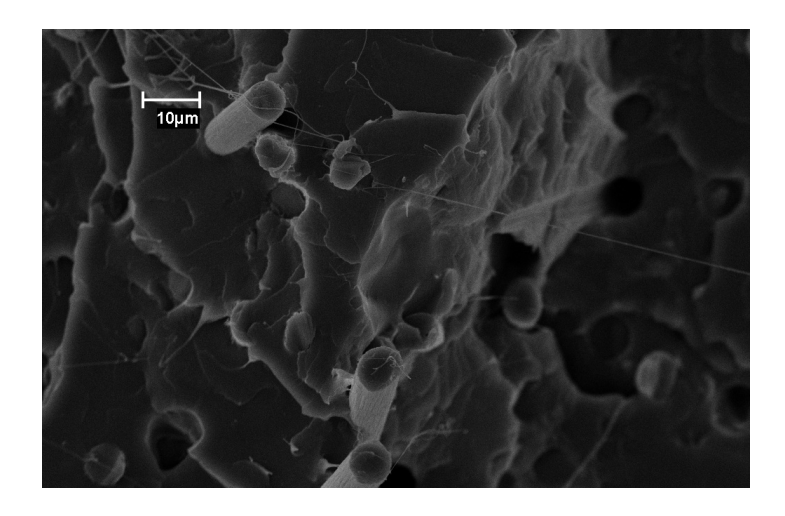


Figure 8: Specimen of PLA+CF at 0° magnified 3000×.

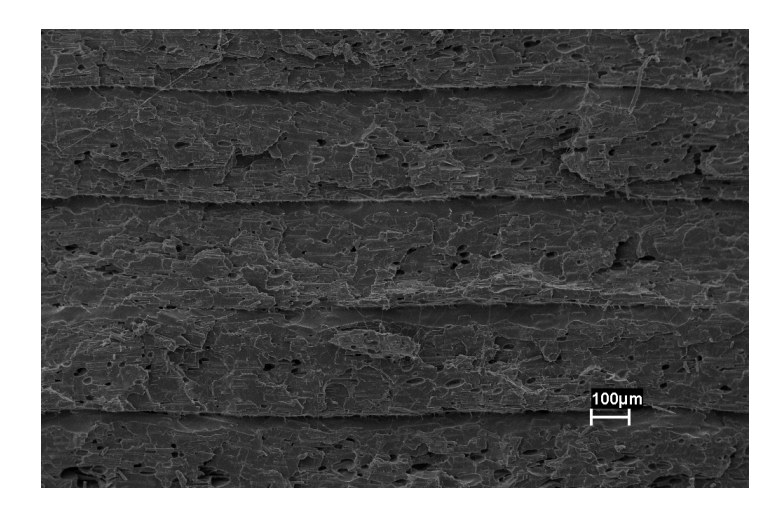


Figure 9: Specimen of PLA+CF at 90° magnified $200\times$.

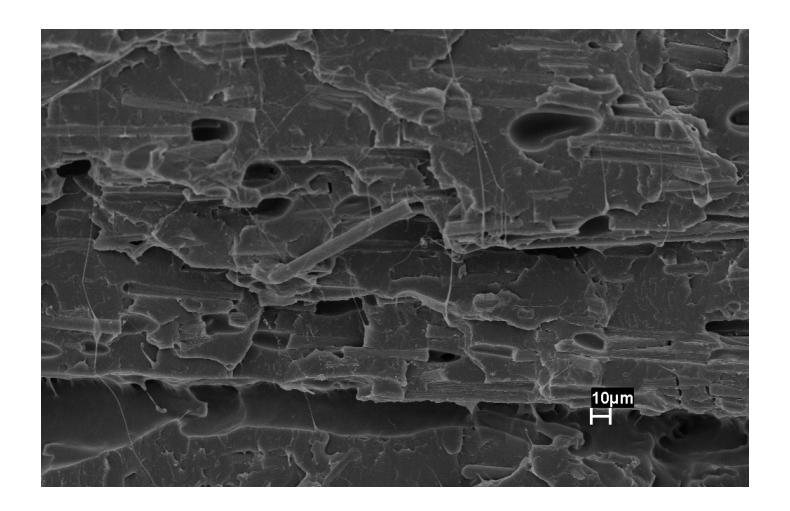


Figure 10: Specimen of PLA+CF at 90° magnified 1000×.

Figures 9 and 10 show, with increasing magnification, the fracture surface of the PLA+CF specimen printed at 90° . In Fig.9, with magnification of $200\times$, it is possible to see laterally the material lines deposited by FFF. In Fig.10, with magnification of $1000\times$, it is possible to see carbon fibers and also voids with shapes resembling cylinders. The latter are result of the fiber pull-outs during failure of the specimen, while tested by a tensile load applied perpendicularly to the material deposition direction. Other voids, which are not result of fiber pull-outs, are noticed as in other images.

Figures 11 and 12 show, with increasing magnification, the fracture surface of the PLA+CF specimen printed at $\pm 45^{\circ}$. In Fig.11, with magnification of $200\times$, it is possible to notice the crossed deposition directions of the printed material lines. In Fig.12, with magnification of $1000\times$, it is possible to see the reinforcing carbon fibers, the voids left by fiber pull-outs and other voids, in the same manner as observed earlier.

At this point it is very important to highlight, from the SEM images of the PLA+CF specimens, that the short carbon fibers dispersed in the PLA matrix showed up to be highly oriented with the printing directions. This can be easily observed, specially from Fig.7, 10 and 12, where the printing directions were respectively 0°, 90° and ±45°. This is the fact that explains the differences in stiffnesses noticed in the results of Tab.3 and 4. It can be concluded that the PLA+CF printed material has a stiffness behavior similar to unidirectional fiber reinforced composites, once it is indeed a composite reinforced with short fibers which ended up highly oriented with the printing direction after production by FFF. One may ask if these fibers were oriented during the FFF deposition process or if the fibers were already oriented in the filament loaded in the 3D printer. This important question will be answered in the following Sec.5.

Regarding to the number of fiber pull-outs seen in Figs.7, 10 and 12, which respectively show specimens printed at 0° , 90° and $\pm 45^{\circ}$, it can be said that it is relatively big, which is explained by the poor adhesion between PLA and carbon fibers already commented.

Finishing the discussion about SEM micrographs of the tested specimens, Fig.13 and 14 show, with increasing magnification, the fracture surfaces of the PLA specimen printed at 0°. Fig.13, with magnification of 200×, shows details of the periodic microstructure of the material produced by FFF, including triangular shaped voids left by the process. The latter described figure and Fig.14, with magnification of 3000×, shows that the production of the PLA specimens by FFF did not left voids inside the material deposited lines, as occurred with the PLA+CF.

5 SEM of the PLA+CF filament

Figures 15 and 16 are micrographs obtained by SEM, showing the cross section of a sample of the PLA+CF 3D printing filament employed in this study.

From Fig.15, with magnification of $200\times$, it is possible to see the round shape of the filament cross section, whose nominal diameter is 1.75 mm. In Fig.16, with magnification of $1000\times$, it is possible to notice the same elements found in the previous micrographs: carbon fibers, voids left by fiber pull-outs (the watched sample was separated from its spool with a blade, removing some fibers from the cut surface) and other voids.

It is clearly seen that the filament has the short carbon fibers mostly oriented with the direction of its length (the two fibers seen in the plane of the cross section were probably left there after sample's cutting). Therefore, it can be safely assumed that the carbon fibers were aligned within the feeding filament and remained aligned in the tested specimens produced by the FFF process.

This behavior can be explained by the fact that, during 3D printing, the PLA is melt down by the extrusion nozzle and the fibers inside the deposited material have a trend to become aligned with the extrusion direction of the molten thermoplastic. This behavior was already reported in the literature [49, 38] for ABS reinforced with short carbon fibers, and is now also observed for PLA. However, in an injection molded PLA with addition of very short carbon nanofibers at [50] this was not observed, leading to conclude that this alignment is function of the production process and possibly of the fibers geometry.

The voids that are not related to fiber pull-outs are also seen in the PLA+CF filament, not only in the microstructure of the produced specimens as seen in the previous Sec.4. As said before, the reason for the appearance of these voids is an open subject.

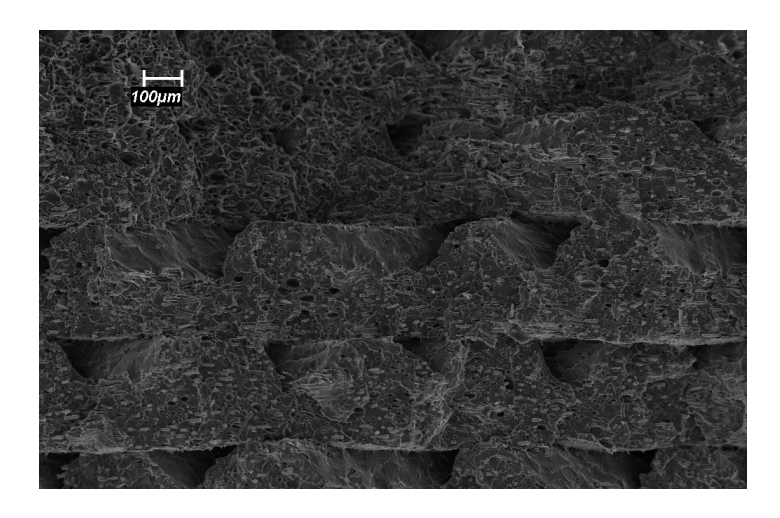


Figure 11: Specimen of PLA+CF at $\pm 45^{\circ}$ magnified 200×.

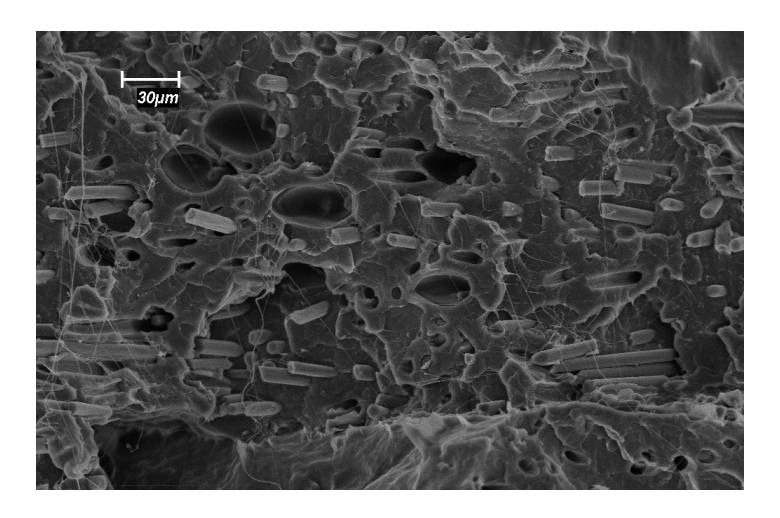


Figure 12: Specimen of PLA+CF at $\pm 45^{\circ}$ magnified 1000×.

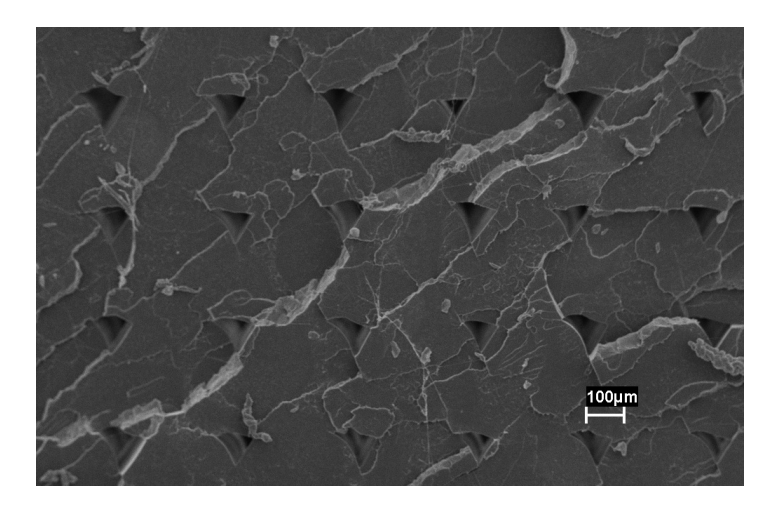


Figure 13: Specimen of PLA at 0° magnified $200\times.$

6 Short fibers length estimation

A final but very important comment regards to the length of the short carbon fibers in PLA+CF. From the scales of Fig.10 and 16, the lateral fiber voids and fibers themselves seen in both images, the chopped carbon fibers that reinforce the PLA+CF can have their length estimated in an average of 60 μm . These fibers are shorter than the fibers used as reinforcement in previous works: about 100 μm in [49], 200 μm to 400 μm in [38] and 100 μm to 150 μm in [31].

Longer fibers have bigger external surface areas, which may improve fiber-matrix adhesion. In [49], [38] and [31], this can explain the increase in both stiffnesses and strengths of ABS composites. In the present work, the fibers did not improve the PLA+CF strength (as discussed in Sec.3). Reasons seem to be the poor adhesion between PLA and carbon fibers, already reported in the literature [43, 47], and the length of the reinforcing fibers, perhaps too short (with small external contact surface area), also not collaborating to fiber-matrix adhesion. In [50], nanofibers of length below 4 μm (very short) were not able to improve strengths in an injection molded PLA composite as well. However, the present authors do not know if the adhesion between PLA and carbon fibers is good enough to make beneficial the use of longer chopped fibers in their composites, with respect to final mechanical properties.

7 Conclusions

This work presents results for mechanical testing and SEM micrography of materials produced by 3D printing based on FFF. Two printing materials were investigated, a PLA and a PLA+CF (reinforced with short carbon fibers of length about $60~\mu m$ in a weight fraction of 15%). The specimens were all printed with material deposition specially oriented (at 0° , 90° or $\pm 45^{\circ}$), with constant microstructure and same build parameters.

From the results presented for stiffnesses, it can be concluded that the short carbon fibers increased a lot (about 2.2 times) the tensile modulus E_1 (respective to the printing direction) of the reinforced PLA+CF, in comparison to the same property of the PLA. The tensile modulus E_2 (transverse to the printing direction) and the shear modulus G_{12} (respective to the plane of printing) were also increased by the short fibers, respectively 1.25 and 1.16 times, therefore not as much as E_1 was. Moreover, the reinforcing fibers let the Poisson coefficients ν_{12} and ν_{21} of the PLA+CF distant from each other (ν_{12} was 2.5 times higher than ν_{21}), an expected result based on the increase in E_1 stiffness of the PLA+CF.

The tests performed also rendered materials strengths: the tensile strengths S_1^* (with respect to the printing direction) and S_2^* (transverse to the printing direction), and the shear strength S_{12}^* (respective to the plane of printing). Comparing results for the PLA and PLA+CF, it was noticed that the short carbon fibers practically did not alter such quantities. It can be thought that the PLA matrix carried out the majority of the stresses at the failure load level in both the PLA and PLA+CF.

The length of the chopped fibers in PLA+CF was estimated in $60 \mu m$, maybe too short for consistently improving strengths. A complication factor for the present case is the poor adhesion between PLA and carbon fibers, already reported in the literature [43, 47]. Failure in PLA+CF happened at lower strains than in PLA, indicating that the reinforced material became more brittle with the addition of short carbon fibers.

The SEM of the PLA+CF revealed that the short carbon fibers in this composite were mostly aligned with the length of the 3D printing filament, inside this feeding material, and remained aligned with the direction of printing within the specimens produced by FFF. Due to this, the biggest increase in stiffness for the PLA+CF happened in the direction of printing.

The present comments explain differences in stiffnesses and strengths for the PLA and PLA+CF.

8 Acknowledgements

This work was supported by grants from ITA T-61 and FAPESP Process 2015/00159-5.

A Note on PLA printing temperature

The PLA material employed in this work was, in initial tests, printed at $220^{\circ}C$ by recommendation of the filament producer, found at the product spool. However, it was noticed that this printing temperature caused small bubble-like structures in the specimens, as later confirmed by chromatic aberrations confocal microscopy (thanks to the equipment Cyber CT 100 at the Centre of Competence in Manufacturing CCM/ITA). The authors believed that this could indicate that the printing temperature was too high. A temperature of $190^{\circ}C$ (common for printing PLA) was then tested, and the cited microscopy technique indicated that the bubble-like structures disappeared from the printed specimens, showing that this was indeed more appropriate. Fig.17 shows the acquired micrographs that led to this conclusion.

References

- [1] J. M. Pearce, Applications of open source 3D printing on small farms, Organic Farming 1 (1) (2015) 19–35. doi:10.12924/of2015.01010019.
- [2] M. Vaezi, S. Yang, Extrusion-based additive manufacturing of PEEK for biomedical applications, Virtual and Physical Prototyping 10 (3) (2015) 123–135. doi:10.1080/17452759.2015.1097053.
- [3] F. S. Senatov, K. V. Niaza, A. A. Stepashkin, S. D. Kaloshkin, Low-cycle fatigue behavior of 3D-printed PLA-based porous scaffolds, Composites Part B 97 (2016) 193 200. doi:10.1016/j.compositesb.2016.04.067.
- [4] R. Munhoz, C. A. da Costa Moraes, H. Tanaka, M. E. Kunkel, A digital approach for design and fabrication by rapid prototyping of orthosis for developmental dysplasia of the hip, Research on Biomedical Engineering 32 (1) (2016) 63–73. doi:10.1590/2446-4740.00316.
- [5] G. D. Goh, S. Agarwala, G. L. Goh, V. Dikshit, S. L. Sing, W. Y. Yeong, Additive manufacturing in unmanned aerial vehicles (UAVs): challenges and potential, Aerospace Science and Technology 63 (2017) 140–151. doi:10.1016/j.ast.2016.12.019.
- [6] C. Ferro, R. Grassi, C. Secli, P. Maggiore, Additive manufacturing offers new opportunities in UAV research, Procedia CIRP 41 (2016) 1004–1010. doi:10.1016/j.procir.2015.12.104.
- [7] D. Sundaramurthi, S. Rauf, C. Hauser, 3D bioprinting technology for regenerative medicine applications, International Journal of Bioprinting 2 (2) (2016) 9–26. doi:10.18063/IJB.2016.02.010.
- [8] C. Murphy, K. Kolan, W. Li, J. Semon, D. Day, M. Leu, 3D bioprinting of stem cells and polymer/bioactive glass composite scaffolds for bone tissue engineering, International Journal of Bioprinting 3 (1) (2017) 1–11. doi:10.18063/IJB.2017.01.005.
- [9] J. Y. Lee, W. S. Tan, J. An, C. K. Chua, C. Y. Tang, A. G. Fane, T. H. Chong, The potential to enhance membrane module design with 3D printing technology, Journal of Membrane Science 499 (2016) 480–490. doi:10.1016/j.memsci.2015.11.008.
- [10] D. Appleyard, Powering up on powder technology, Metal Powder Report 70 (6) (2015) 285–289. doi:10.1016/j.mprp.2015.08.075.
- [11] M. Invernizzi, G. Natale, M. Levi, S. Turri, G. Griffini, UV-assisted 3D printing of glass and carbon fiber-reinforced dual-cure polymer composites, Materials 9 (7) (2016) 583 (1–12). doi: 10.3390/ma9070583.
- [12] I. Hager, A. Golonka, R. Putanowicz, 3D printing of buildings and building components as the future of sustainable construction?, Procedia Engineering 151 (2016) 292–299. doi:10.1016/j.proeng.2016.07.357.

- [13] I. Farina, F. Fabbrocino, G. Carpentieri, M. Modano, A. Amendola, R. Goodall, L. Feo, F. Fraternali, On the reinforcement of cement mortars through 3D printed polymeric and metallic fibers, Composites Part B 90 (2016) 76–85. doi:10.1016/j.compositesb.2015.12.006.
- [14] I. Farina, F. Fabbrocino, F. Colangelo, L. Feo, F. Fraternali, Surface roughness effects on the reinforcement of cement mortars through 3D printed metallic fibers, Composites Part B 99 (2016) 305 – 311. doi:10.1016/j.compositesb.2016.05.055.
- [15] R. Hahnlen, M. J. Dapino, NiTi-Al interface strength in ultrasonic additive manufacturing composites, Composites Part B 59 (2014) 101 108. doi:10.1016/j.compositesb.2013.10.024.
- [16] A. Hehr, M. J. Dapino, Interfacial shear strength estimates of NiTi-Al matrix composites fabricated via ultrasonic additive manufacturing, Composites Part B 77 (2015) 199 208. doi:10.1016/j.compositesb.2015.03.005.
- [17] J. Li, T. Monaghan, T. Nguyen, R. Kay, R. Friel, R. Harris, Multifunctional metal matrix composites with embedded printed electrical materials fabricated by ultrasonic additive manufacturing, Composites Part B 113 (2017) 342 354. doi:10.1016/j.compositesb.2017.01.013.
- [18] P. Tran, T. D. Ngo, A. Ghazlan, D. Hui, Bimaterial 3D printing and numerical analysis of bioinspired composite structures under in-plane and transverse loadings, Composites Part B 108 (2017) 210 – 223. doi:10.1016/j.compositesb.2016.09.083.
- [19] J. Sun, Z. Peng, L. Yan, J. Y. H. Fuh, G. S. Hong, 3D food printing an innovative way of mass customization in food fabrication, International Journal of Bioprinting 1 (1) (2015) 27–38. doi:10.18063/IJB.2015.01.006.
- [20] L. E. Murr, Frontiers of 3D printing/additive manufacturing: from human organs to aircraft fabrication, Journal of Materials Science and Technology 32 (10) (2016) 987–995. doi:10.1016/ j.jmst.2016.08.011.
- [21] S. Upcraft, R. Fletcher, The rapid prototyping technologies, Assembly Automation 23 (4) (2003) 318–330. doi:10.1108/01445150310698634.
- [22] C. K. Chua, K. F. Leong, 3D printing and additive manufacturing: principles and applications, 5th Edition, World Scientific Publishing Company, Singapore, 2017. doi:10.1142/9789814578486_fmatter.
- [23] P. Kulkarni, D. Dutta, Deposition strategies and resulting part stiffnesses in fused deposition modeling, Journal of Manufacturing Science and Engineering 121 (1) (1999) 93–103. doi:10. 1115/1.2830582.
- [24] A. K. Sood, R. K. Ohdar, S. S. Mahapatra, Parametric appraisal of mechanical property of fused deposition modelling processed parts, Materials and Design 31 (1) (2010) 287–295. doi: 10.1016/j.matdes.2009.06.016.
- [25] O. A. Mohamed, S. H. Masood, , J. L. Bhowmik, Optimization of fused deposition modeling process parameters: a review of current research and future prospects, Advanced Manufacturing 3 (2015) 42–53. doi:10.1007/s40436-014-0097-7.
- [26] R. Singh, P. Bedi, F. Fraternali, I. Ahuja, Effect of single particle size, double particle size and triple particle size Al2O3 in Nylon-6 matrix on mechanical properties of feed stock filament for FDM., Composites Part B 106 (2016) 20 – 27. doi:10.1016/j.compositesb.2016.08.039.
- [27] K. Boparai, R. Singh, F. Fabbrocino, F. Fraternali, Thermal characterization of recycled polymer for additive manufacturing applications, Composites Part B 106 (2016) 42 47. doi:10.1016/j.compositesb.2016.09.009.

- [28] R. Singh, N. Singh, A. Amendola, F. Fraternali, On the wear properties of Nylon6-SiC-Al2O3 based fused deposition modelling feed stock filament, Composites Part B 119 (2017) 125 131. doi:10.1016/j.compositesb.2017.03.042.
- [29] W. Zhong, F. Li, Z. Zhang, L. Song, Z. Li, Short fiber reinforced composites for fused deposition modeling, Materials Science and Engineering A 301 (2) (2001) 125–130. doi:10.1016/S0921-5093(00)01810-4.
- [30] F. V. Klift, Y. Koga, A. Todoroki, M. Ueda, Y. Hirano, R. Matsuzaki, 3D printing of continuous carbon fibre reinforced thermo-plastic (CFRTP) tensile test specimens., Open Journal of Composite Materials 6 (2016) 18–27. doi:10.4236/ojcm.2016.61003.
- [31] F. Ning, W. Cong, J. Qiu, J. Wei, S. Wang, Additive manufacturing of carbon fiber reinforced thermoplastic composites using fused deposition modeling, Composites Part B 80 (2015) 369–378. doi:10.1016/j.compositesb.2015.06.013.
- [32] M. Chapiro, Current achievements and future outlook for composites in 3D printing, Reinforced Plastics 60 (6) (2016) 372–375. doi:10.1016/j.repl.2016.10.002.
- [33] X. Wang, M. Jiang, Z. Zhou, J. Gou, D. Hui, 3D printing of polymer matrix composites: a review and prospective, Composites Part B 110 (2017) 442–458. doi:10.1016/j.compositesb.2016. 11.034.
- [34] S.-H. Ahn, M. Montero, D. Odell, S. Roundy, P. K. Wright, Anisotropic material properties of fused deposition modeling ABS, Rapid Prototyping Journal 8 (4) (2002) 248–257. doi:10.1108/ 13552540210441166.
- [35] A. Bellini, S. Güçeri, Mechanical characterization of parts fabricated using fused deposition modeling, Rapid Prototyping Journal 9 (4) (2003) 252–264. doi:10.1108/13552540310489631.
- [36] R. Zou, Y. Xia, S. Liu, P. Hu, W. Hou, Q. Hu, C. Shan, Isotropic and anisotropic elasticity and yielding of 3D printed material, Composites Part B 99 (2016) 506 513. doi:10.1016/j.compositesb.2016.06.009.
- [37] G. Alaimo, S. Marconi, L. Costato, F. Auricchio, Influence of meso-structure and chemical composition on FDM 3D-printed parts, Composites Part B 113 (2017) 371-380. doi:10.1016/j.compositesb.2017.01.019.
- [38] H. L. Tekinalp, V. Kunc, G. M. Velez-Garcia, C. E. Duty, L. J. Love, A. K. Naskar, C. A. Blue, S. Ozcan, Highly oriented carbon fiber-polymer composites via additive manufacturing, Composites Science and Technology 105 (2014) 144-150. doi:10.1016/j.compscitech.2014. 10.009.
- [39] L. J. Love, V. Kunc, O. Rios, C. E. Duty, A. M. Elliott, B. K. Post, R. J. Smith, C. A. Blue, The importance of carbon fiber to polymer additive manufacturing, Journal of Materials Research 29 (17) (2014) 1893–1898. doi:10.1557/jmr.2014.212.
- [40] F. Ning, W. Cong, Y. Hu, H. Wang, Additive manufacturing of carbon fiber-reinforced plastic composites using fused deposition modeling: effects of process parameters on tensile properties, Journal of Composite Materials 51 (4) (2016) 451–462. doi:10.1177/0021998316646169.
- [41] S. A. Hinchcliffe, K. M. Hess, W. V. Srubar-III, Experimental and theoretical investigation of prestressed natural fiber-reinforced polylactic acid (PLA) composite materials, Composites Part B 95 (2016) 346–354. doi:10.1016/j.compositesb.2016.03.089.
- [42] M. Ho, H. Wang, J.-H. Lee, C. Ho, K. Lau, J. Leng, D. Hui, Critical factors on manufacturing processes of natural fibre composites, Composites Part B 43 (8) (2012) 3549-3562. doi:10.1016/ j.compositesb.2011.10.001.

- [43] N. Li, Y. Li, S. Liu, Rapid prototyping of continuous carbon fiber reinforced polylactic acid composites by 3D printing, Journal of Materials Processing Technology 238 (2016) 218–225. doi: 10.1016/j.jmatprotec.2016.07.025.
- [44] T. Yu, J. Ren, S. Li, H. Yuan, Y. Li, Effect of fiber surface-treatments on the properties of polylactic acid/ramie composites, Composites Part A 41 (4) (2010) 499-505. doi:10.1016/j. compositesa.2009.12.006.
- [45] X. Yao, C. Luan, D. Zhang, L. Lan, J. Fu, Evaluation of carbon fiber-embedded 3D printed structures for strengthening and structural-health monitoring, Materials and Design 114 (4) (2017) 424–432. doi:10.1016/j.matdes.2016.10.078.
- [46] X. Tian, T. Liu, C. Yang, Q. Wang, D. Li, Interface and performance of 3D printed continuous carbon fiber reinforced PLA composites, Composites Part A 88 (2016) 198–205. doi:10.1016/ j.compositesa.2016.05.032.
- [47] X. Tian, T. Liu, Q. Wang, A. Dilmurat, D. Li, G. Ziegmann, Recycling and remanufacturing of 3D printed continuous carbon fiber reinforced PLA composites, Journal of Cleaner Production 142 (2017) 1609–1618. doi:10.1016/j.jclepro.2016.11.139.
- [48] G. W. Melenka, B. K. Cheung, J. S. Schofield, M. R. Dawson, J. P. Carey, Evaluation and prediction of the tensile properties of continuous fiber-reinforced 3D printed structures, Composite Structures 153 (2016) 866–875. doi:10.1016/j.compstruct.2016.07.018.
- [49] M. L. Shofner, K. Lozano, F. J. Rodriguez-Macias, E. V. Barrera, Nanofiber-reinforced polymers prepared by fused deposition modeling, Journal of Applied Polymer Science 89 (2003) 3081–3090. doi:10.1002/app.12496.
- [50] M. A. Anwer, H. E. Naguib, Study on the morphological, dynamic mechanical and thermal properties of PLA carbon nanofibre composites, Composites Part B 91 (2016) 631–639. doi:10.1016/j.compositesb.2016.01.039.
- [51] American Society for Testing and Materials, Standard test method for tensile properties of plastics. ASTM D638-10 (2010). doi:10.1520/D0638-10.
- [52] American Society for Testing and Materials, Standard test method for in-plane shear response of polymer matrix composite materials by tensile test of a +-45 laminate. ASTM D3518-13 (2013). doi:10.1520/D3518_D3518M.
- [53] A. Jaszkiewicz, A. Meljon, A. Bledzki, M. Radwanski, Gaining knowledge on the processability of PLA-based short-fibre compounds a comprehensive comparison with their PP counterparts, Composites Part A 83 (2016) 140–151. doi:10.1016/j.compositesa.2015.09.022.
- [54] S. Farah, D. G. Anderson, R. Langer, Physical and mechanical properties of PLA, and their functions in widespread applications - a comprehensive review, Advanced Drug Delivery Reviews 107 (2016) 367–392. doi:10.1016/j.addr.2016.06.012.
- [55] M. Murariu, P. Dubois, PLA composites: from production to properties, Advanced Drug Delivery Reviews 107 (2016) 17–46. doi:10.1016/j.addr.2016.04.003.
- [56] C. C. Kuo, L. C. Liu, W. F. Teng, H. Y. Chang, F. M. Chien, S. J. Liao, W. F. Kuo, C. M. Chen, Preparation of starch/acrylonitrile-butadiene-styrene copolymers (ABS) biomass alloys and their feasible evaluation for 3D printing applications, Composites Part B 86 (2016) 36–39. doi: 10.1016/j.compositesb.2015.10.005.
- [57] J. N. Reddy, Mechanics of laminated composite plates: theory and analysis, CRC Press, Boca Raton, 1997, ISBN 9780849331015.

- [58] A. E. Lam, Analysis of mechanical strength of components fabricated by the process of fused deposition modelling FDM, Master's thesis, Aeronautics Institute of Technology, São José dos Campos, São Paulo, Brazil (2008).
 URL http://www.bdita.bibl.ita.br/tesesdigitais/verifica_session.php?num_tese= 000552470&origem=BDITA
- [59] B. M. Tymrak, M. Kreiger, J. M. Pearce, Mechanical properties of components fabricated with open-source 3D printers under realistic environmental conditions, Materials and Design 58 (2014) 242–246. doi:10.1016/j.matdes.2014.02.038.

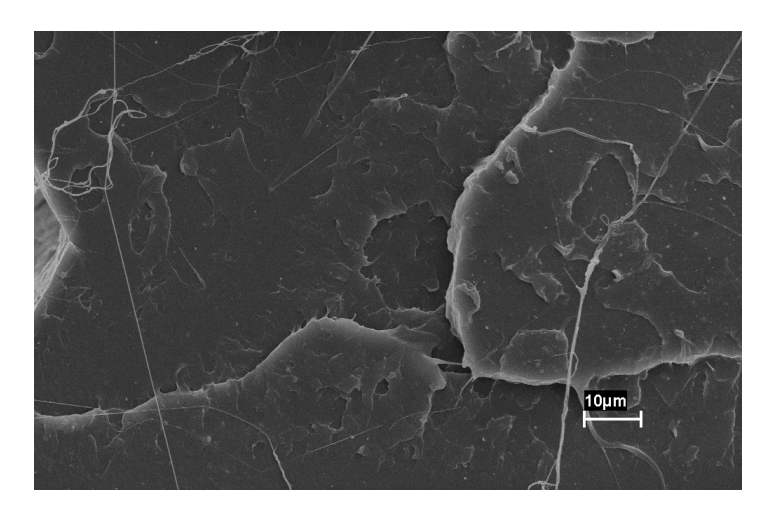


Figure 14: Specimen of PLA at 0° magnified $3000 \times$.

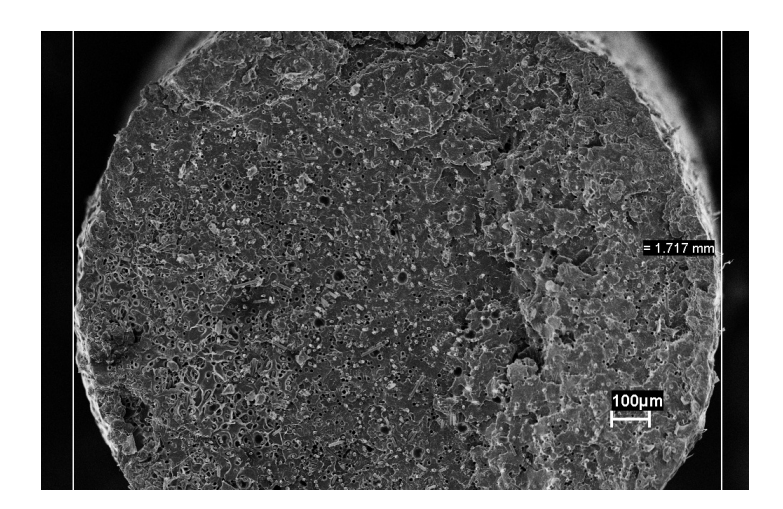


Figure 15: Cross section of the PLA+CF filament magnified 200 \times .

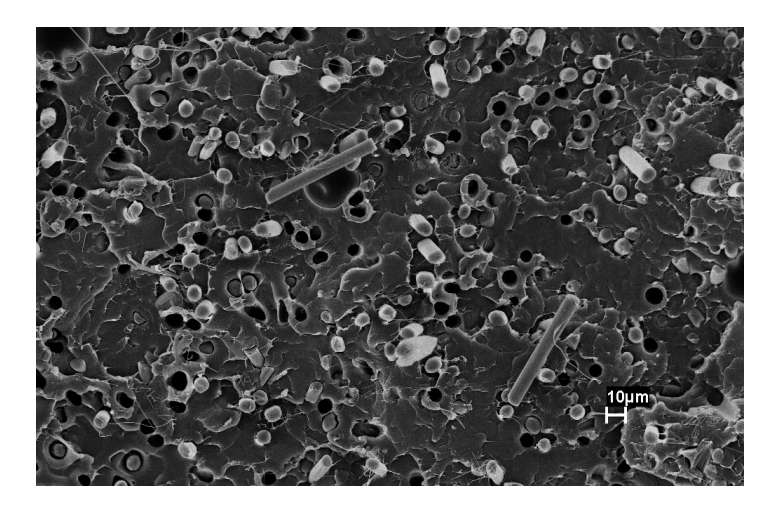


Figure 16: Cross section of the PLA+CF filament magnified 1000×.

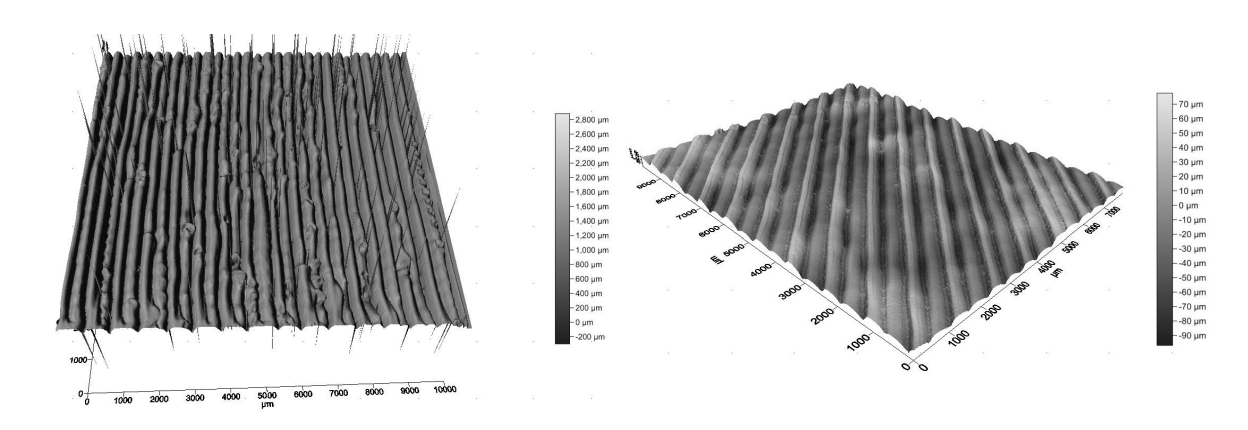


Figure 17: PLA printed at $220^{\circ}C$ (left, with bubble-like structures) and at $190^{\circ}C$ (right, without bubble-like structures).